ELSEVIER

Ceramics International 25 (1999) 447–454

CERAMICS INTERNATIONAL

Fracture toughness of structural ceramics

A.K. Mukhopadhyay [a,*], S.K. Datta [b], D. Chakraborty [a]

[a] *Central Glass and Ceramic Research Institute, Calcutta 700 032, India*
[b] *Khanakul College, Hoogli, West Bengal, India*

Received 30 March 1998; accepted 1 July 1998

Abstract

A comparative study of fracture toughness evaluation at room temperature of three different structural ceramics viz. sintered alumina, silicon carbide and silicon nitride is reported. Four methods of fracture toughness evaluation such as the single edge notched beam (SENB) technique, chevron notched beam (CNB) technique, indentation fracture (IF) technique and fractographic methods (FM) were compared. In addition, for a given method, the influence of several experimental parameters, e.g. blade width, notch tip radius, normalised notch length and the loading rate on the measured value of fracture toughness was investigated in the cases of the aforesaid materials.

1. Introduction

A unique, unambiguous, universally acceptable method to evaluate fracture toughness (K_{1c}) of structural ceramics is yet to emerge. This has led various researchers to adopt different methods to evaluate fracture toughness of materials. For instance, Chen and Ardell [1] have recently proposed a miniaturised disk bend test (MDBT) for evaluation of K_{1c} in the cases where small amount of material is available. Their data on silicon carbide and nitride ceramics as well as other materials were found to be comparable to data evaluated by other conventional methods. Haubensk [2] has recently advocated a new method namely, measurement of crack opening displacement (COD) to measure fracture toughness of porous reaction bonded silicon nitride ceramics. The indentation fracture method has been applied to alumina–hydroxyapatite (HAP) particulate composite, alumina–silicon carbide particulate nanocomposites as well as to high alumina (85%) ceramics [3–5]. In the case of 6061Al–SiC metal matrix composites (MMC) however, the conventional single edge notched beam (SENB) method has been applied under three point loading [6]. It has been recently shown that in the case of nickel–alumina composites the K_{1c} values obtained by the chevron notched bar (CNB) technique from the peak load and the work of fracture considerations are different from each other and both these methods predict values higher than the toughness value at the crack initiation point [7]. Nojima et al. have utilised compact tension (CT) specimens for evaluation of K_{1c} in the cases of alumina as well as soda lime glass materials recently [8]. In the case of polymeric composites e.g. 52 vol% E-glass fibers in a M-10 epoxy matrix, both double cantilever beam (DCB) and edge loaded split beam (ELS) techniques have been utilised to evaluate delamination fracture toughness [9]. Rice has recently shown very explicitly the complex nature and degree of dependence of fracture toughness on such important microstructural parameters as grain size and porosity of several important ceramics including alumina [10]. This particular work highlights the need to develop better understanding about the micromechanics of fracture initiation in the perspective of inhomogeniety normally encountered in the microstructure of common structural ceramics. Clearly one can find a large variety of materials–methodologies combination, as far as the problem of fracture toughness evaluation is concerned. More often than not, the methods adapted from the techniques already in practice for the metallic materials, have led to controversial results in the case of structural ceramics [11,12]. There is ample evidence in literature that the evaluated value of K_{1c} is sensitive to the method of measurement as well as to the experimental parameters of a given method [13–16]. Such issues assume even greater significance than before because of the presence of a rising crack growth resistance curve (R-curve) behaviour in a variety of structural

* Corresponding author.

0272-8842/99/$20.00
PII: S0272-8842(98)00056-X

ceramics [1,8,10]. The purpose of the present work was (i) to compare four methods of K_{1c} evaluation, e.g. single edge notched beam (SENB) technique, chevron notched beam (CNB) technique, indentation fracture (IF) technique and fractographic method (FM); and (ii) to study for a given method, the influence of experimental parameters viz. blade width ($B \sim 0.05$–0.30 mm), notch tip radius ($\rho \sim 100$–300 μm), normalised notch length ($a/W \sim 0.1$–0.6) and the loading rate (0.015–0.150 $MPas^{-1}$) on the measured value of K_{1c}. The materials chosen were sintered alumina, silicon carbide and silicon nitride.

2. Materials and methods

The alumina samples (A,D1,E,F) were obtained as sintered products from commercial vendors (M/s Wade, UK). The sintered silicon carbide (SiC) was also commercially obtained (M/s Grindwell Norton India Pvt. Ltd.). The sintered silicon nitride (SSN) samples were prepared in the laboratory [17]. The chemical analysis data of various sintered alumina ceramics are given in Table 1. The nominal compositional details of the SSN ceramics are given in Table 2. The silicon nitride powder utilised in fabrication of SSN was synthesised in the laboratory [17]. Phase purity of the alumina and silicon carbide ceramics was checked by conventional X-ray diffraction (XRD) technique (Fig. 1). The microstructural data of the various structural ceramics investigated in the present work, are given in Table 3. The grain size was estimated from polished and thermally etched sections using a image analyser which had a precision of beterr than ± 0.01 μm. Density was estimated by Archimedes' principle. Volume percent of open porosity was estimated from the measured density value. The theoretical density values were taken from literature for the alumina and silicon carbide ceramics. In the case of SSN ceramics it was calculated taking into consideration the various sintering additives utilised in their preparation. Typical microstructures of the alumina and SSN ceramics are shown in Fig. 2. Attempts to obtain good quality micrograph for the porous SiC ceramic were not quite successful.

The rectangular, tensile surface polished (center line average ˜ 1 μm) specimens ($45 \times 4.5 \times 3.5$ mm), used for evaluation of K_{1c} by the SENB and CNB techniques were all tested in a universal testing machine (Instron, 1185) at room temperature under ambient laboratory conditions with four point loading configuration using a jig made out of sintered silicon carbide [17]. All K_{1c} (SENB) data were obtained following ASTM specifications and formulations [18]. K_{1c} (CNB) data were obtained following the work of Munz and co-workers [19,20], with a relative notch depth (α_0) of 0.2 and $\alpha_1 \sim 1$ and corrected for deviation of the chevron notch from the mid-thickness plane, as per ASTM recommendations [21]. The evaluation of K_{1c} by indentation technique was done following the work of Anstis et al. [22] and independent experimental determination of hardness and Young's moduli data for all the present materials [23,24]. Measurement of K_{1c} data by the intrinsic flaw fractographic method (FM) involved identification and direct estimation of the critical flaw sizes from the fractured surfaces of test pieces broken in four point loading during strength tests conducted at room temperature as well as at elevated temperatures [17,25,26]. All reported data points are an average of at least four–six experiments. Wherever possible, error bars have been used in the data presentation to signify typical scatter in the data. Typical mechanical properties of some of the present materials are given in Table 4.

3. Results and discussions

The chemical analysis data show that there was significant difference in the silica contents of alumina samples A, E and F (Table 1). The SSN samples A1, B, C1, C2 and C3 were all synthesised from the Y_2O_3–AlN–SiO_2 system with varying amounts of sintering liquid and nitrogen concentration (Table 2). Similarly, the SSN samples D, D2, D3 and D4 were synthesised from the MgO–AlN–SiO_2 system with varying amounts of sintering liquid and nitrogen concentration. However, the SSN sample E1 was synthesised from the conventional MgO–SiO_2 system (Table 2). The alumina sample E had alpha alumina as the major phase [Fig. 3(a)]. The XRD patterns of the alumina samples A, D and F [not shown in Fig. 3(a)] were similar to those of E. However, there was some unconverted Si in the SiC sample [Fig. 3(b)]. The major phase in all the SSN samples were beta silicon nitride [17]. The microstructural data of Table 3 indicate that the alumina sample A had a equiaxed microstructure (aspect ratio, 1.08) but the alumina samples D, E and F had somewhat elongated grain structure (aspect ratio &1.5–2) [Fig. 2(a)–(d)]. The microstructure of the SSN samples consisted of the rod shaped grains of beta silicon nitride with large aspect ratio (& 2–6) [Fig. 2(e) and (f)].

Table 1
Chemical analysis data of alumina ceramics

Samples	Alumina A	Alumina E	Alumina F
Materials (wt%)			
Al_2O_3	96.0	95.5	98.5
SiO_2	3.0	0.60	0.36
Fe_2O_3	trace	0.08	0.02
TiO_2	trace	trace	trace
CaO	trace	0.71	0.11
MgO	0.50	0.50	0.30
K_2O	trace	1.50	0.15
Na_2O	trace	1.05	0.33

Table 2
Composition of SSN ceramics

Sample	Mol% sintering aid in the powder batch				The composition of sintering liquid in batch	
	Y_2O_3	AlN	MgO	SiO_2	(wt%)[b]	N_2 (atom%)[b]
A1	10.0	45.0	–[a]	45.0	11.9	18.60
B	7.7	43.6	–	48.6	12.3	16.10
C1	7.7	43.6	–	48.6	12.3	16.10
C2	7.7	43.6	–	48.6	12.3	16.10
C3	7.7	43.6	–	48.6	12.3	16.10
D	–	32.6	30.4	37.0	20.7	16.00
D2	–	40.0	10.0	50.0	23.1	13.80
D3	–	32.6	30.4	37.0	20.7	16.00
D4	–	40.0	10.0	50.0	23.1	13.80
D5	–	40.0	10.0	50.0	23.1	13.80
E1	–	–	66.7	33.3	9.00	–

[a] Not present in the powder batch as an individual component.
[b] Approximate amount in the powder batch.
B, C1, C2, similar composition, different sintering schedule; C3, produced by post sintering heat treatment of SSN B; D, D3, similar composition; D3, produced by post sintering heat treatment of SSN D; D2, D5, similar composition, different sintering schedule; D4, produced by post sintering heat treatment of SSN D2 [17].

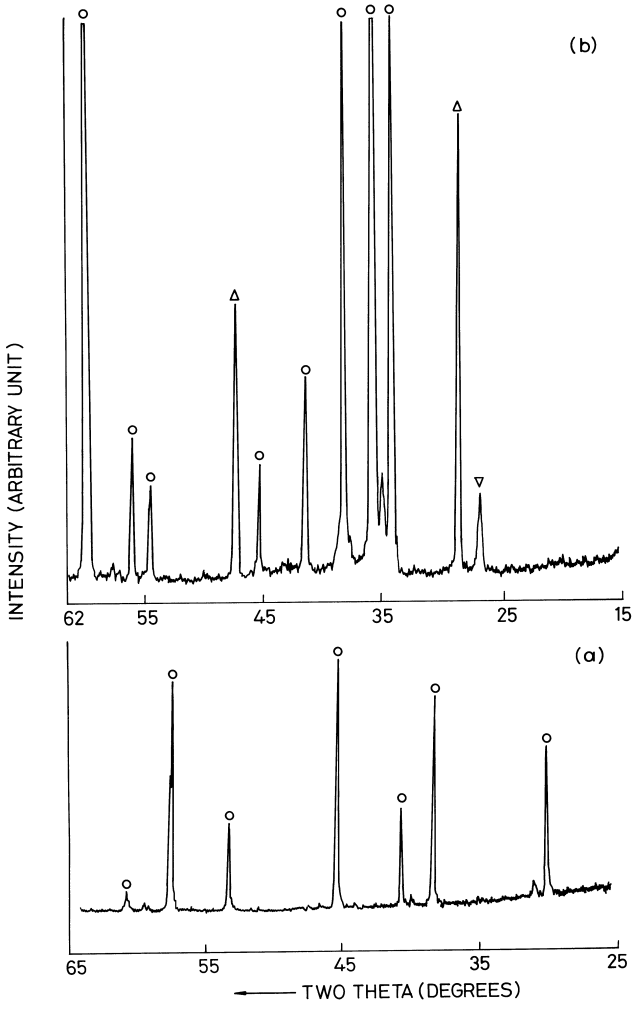

Fig. 1. Typical X-ray diffraction patterns of (a) alumina E (○, α alumina) and (b) SiC ceramics (○, SiC, Δ, Si, ∇, SiO_2).

The data on comparison of K_{1c} values measured by SENB and CNB techniques are shown for Alumina (E,F) and SiC samples in Fig. 3, as a function of blade width (B). For a given material and blade width, K_{1c} (CNB) was always greater than K_{1c} (SENB) for a fixed loading rate of 0.015 MPa s^{-1}. For alumina, similar trend has been reported [27]. However, the present observations for SiC, differ from those of others [19]. A chevron notch is more sharp ended compared to the flat ended notch of a SENB specimen. So, the extent of stable crack extension in a SENB specimen is lesser than that in a CNB specimen. Hence K_{1c} (CNB) is expected to be greater than K_{1c} (SENB), as observed in the present work. Higher K_{1c} (SENB) value of alumina F than alumina E is possibly linked to higher grain size and lower porosity (Fig. 3) as well as higher flexural strength (Fig. 4) of alumina F than those of the alumina E [10]. The SiC samples show the lowest K_{1c} values for a given method (SENB/CNB) and blade width. This may be due to high porosity in the SiC material (Table 3).

The data on comparison of K_{1c} values measured by the SENB, IF and FM techniques are shown for the SSN materials in Fig. 4. All materials taken together, K_{1c} (SENB) is about 1.7 times higher than K_{1c} (IF) [Fig. 4(a)]. Thus, K_{1c} (SENB) is always higher than K_{1c} (IF). Similar trend has been reported for alumina [28]. Lower value of K_{1c} (IF) could be linked to the presence of residual stress field around indentations in SSN [22]. The data of Fig. 4(b) show that in at least 80% cases, K_{1c} (FM) is within 25% of the experimentally measured K_{1c} (SENB) data for SSN samples tested up to moderately high temperature [17]. The slight discrepancy observed between K_{1c} (FM) and K_{1c} (SENB) data in the remaining 20% of the total number of cases investigated in the present work could be ascribed to a combination

Table 3
Microstructural data of alumina, SiC and SSN ceramics

Material	Grain length (L)[a] (μm)	Grain width (B)[a] (μm)	Density (D)[b] (gmcc^{-1})	Vol% open porosity (P)[c]
Alumina A	2.93(0.04)[d]	2.71(0.50)[d]	2.82	28.6
Alumina D1	13.60(1.50)	7.18(0.84)	3.39	14.2
Alumina E	13.04(2.35)	8.89(1.81)	3.31	16.2
Alumina F	17.89(2.15)	11.21(1.46)	3.32	15.9
SiC	4.62(0.91)	2.85(0.59)	2.25	18.7
SSN A1	3.97(0.08)	1.15(0.03)	3.09	3.4
SSN B	2.05(0.04)	0.77(0.02)	3.03	5.3
SSN C1	n.d	n.d	3.03	5.3
SSN C2	2.66(0.05)	0.45(0.03)	3.00	6.2
SSN C3	n.d	n.d	2.84	11.2
SSN D	2.33(0.09)	0.69(0.02)	3.07	4.1
SSN D2	1.68(0.05)	0.73(0.01)	3.01	5.9
SSN D3	1.55(0.66)	0.45(0.03)	3.01	5.9
SSN D4	n.d	n.d	3.12	2.5
SSN D5	n.d	n.d	3.14	1.9
SSN E1	1.80(0.06)	0.58(0.01)	3.03	5.3

[a] Measured by the linear intercept method from SEM photographs of polished and etched sections using a image analyser with a precison of better than ± 0.01 μm.
[b] Measured by water immersion technique following Archimedes principle.
[c] $P=[\{1-(d/d_{th})\}]\times 100$, d_{th} = theoretical density.
[d] Data in parentheses represent ±1 standard deviation.
n.d, not determined.

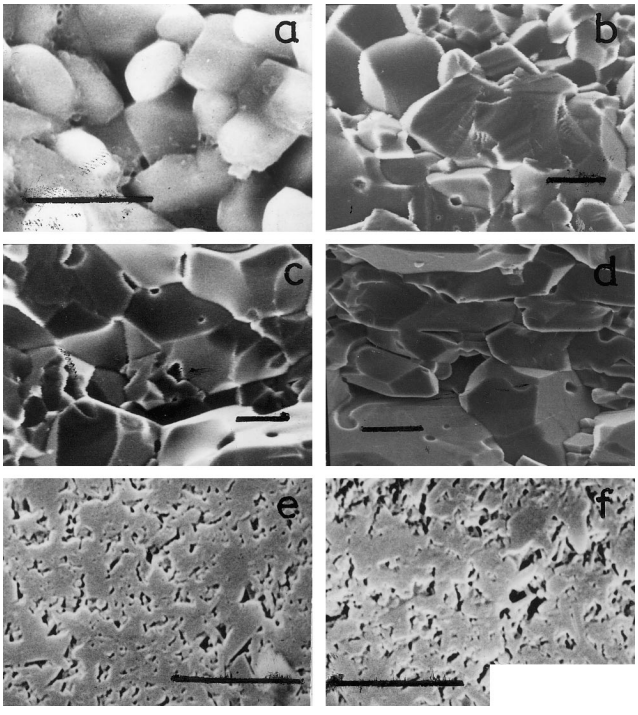

Fig. 2. Typical microstructures of (a) alumina A, fracture surface (scale bar = 5 μm), (b) alumina D1, fracture surface (scale bar = 20 μm), (c) alumina E, fracture surface (scale bar = 10 μm), (d) alumina F, fracture surface (scale bar = 10 μm), (e) SSN A1, polished and thermally etched surface (scale bar = 10 μm), and (f) SSN D, polished and thermally etched surface (scale bar = 10 μm).

Table 4
Mechanical properties at room temperature of alumina, SiC and SSN ceramics

Sample	Fracture toughness (K_{1c}[a]/MPa m$^{1/2}$)	Young's modulus (E[b]/GPa)	Flexural strength (σ[c]/MPa)
Alumina A	2.50	211	195
Alumina E	2.70	244	216
Alumina F	3.22	315	259
SiC	2.51	202	210
SSN A1	7.15	294	502
SSN B	6.01	216	324
SSN D	6.38	237	511
SSN D2	5.48	228	330

[a] SENB technique (4 pt. bend, 40/20, bending arm, 10 mm).
[b] Measured from linear part of load deflection plot using elastic beam theory.
[c] Measured by 4 pt. bend tests (40/20, bending arm, 10 mm), for both K_{1c} (SENB) and σ (4 pt. bend): loading rate 0.015 MPas^{-1} and cross head speed 50 μms^{-1}.

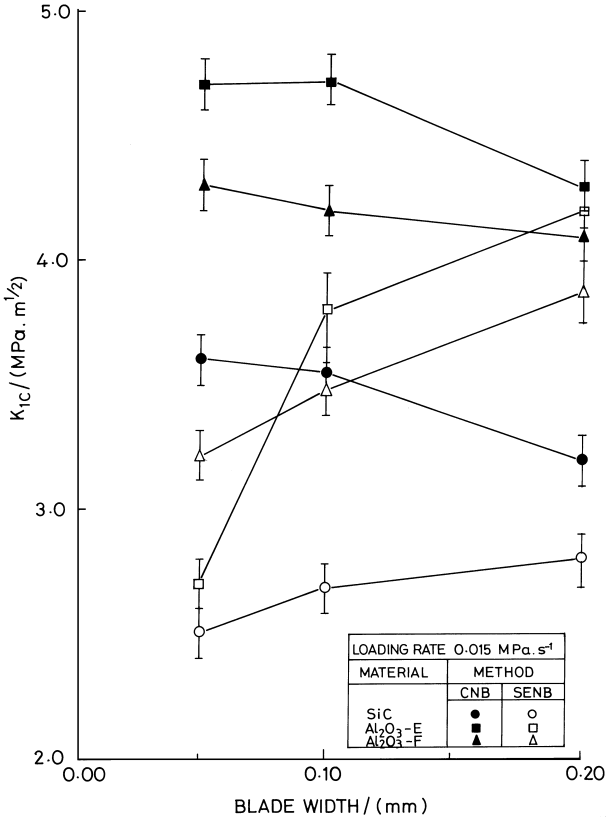

Fig. 3. Comparison of fracture toughness (K_{1c}) data obtained by CNB and SENB techniques applied to alumina and SiC samples at different constant blade widths and a given loading rate.

of several factors: (a) under estimation or over estimation of the measured flaw size as a result of irregularly shaped flaw profile of the observed flaw with the semi-elliptical flaw profile, (b) not taking into consideration the possibility of flaw linking, (c) improper identification of the critical flaw and (d) presence of residual stress [23,29,30].

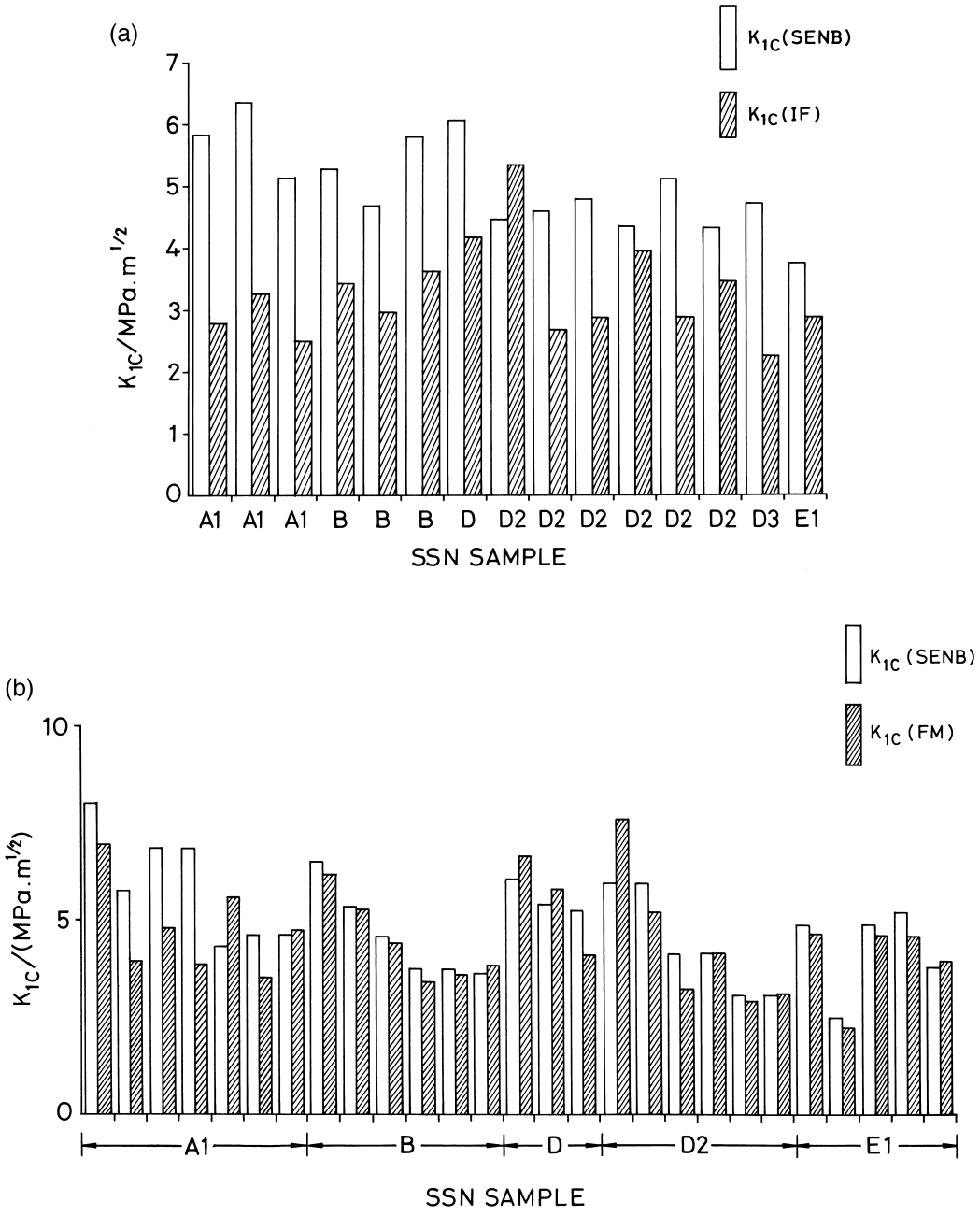

Fig. 4. Comparison of K_{1c} evaluation techniques in the case of SSN samples: (a) SENB vs indentation fracture (IF) method and (b) SENB vs fractographic method (FM).

The data on variation of K_{1c} (SENB) with the width (B) of the blade used for sawing notches are shown for the aluminas A and F in Fig. 5 as a function of loading rates (0.015–0.150 MPa s^{-1}). At any given loading rate, K_{1c} (SENB) of a given alumina sample increases with the blade width. However, for the fine grained alumina, the increasing trend of K_{1c} (SENB) with the blade width somewhat levels off at widths greater than 0.1 mm [Fig. 5(a)]. This trend agrees with that reported by Pabst [31].

Fig. 6 shows the data on influence of loading rate on K_{1c} (SENB) of alumina samples (A,F) with the notches sawn by blades of various widths (0.05–0.30 mm). For a given blade width in a given alumina sample, K_{1c} (SENB) increases with increase in the loading rate. Similar trend has been reported for alumina by Buresch also [32]. However, the effect is more pronounced in the coarse grained alumina [Fig. 6(b)], than in the fine grained alumina [Fig. 6(a)]; as would be expected also from the considerations of *R*-curve behaviour [1,4,7,10]. At faster loading rate, the flaw may not get enough time to grow subcritically. This should limit the critical flaw to a smaller size. The reduction in the critical flaw size may be reflected as an apparent increase in flexural

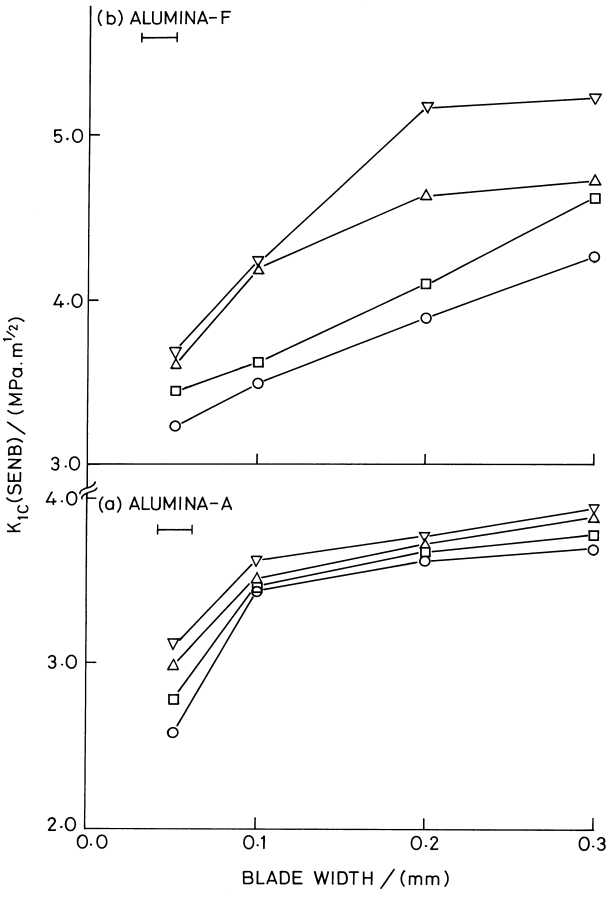

Fig. 5. Variation of K_{1c} (SENB) for alumina ceramics with blade widths (0.05–0.30 mm): (a) alumina A, and (b) alumina F; at different constant loading rates: 0.015 MPas^{-1} (○), 0.03 MPa s^{-1} (□), 0.06 MPa s^{-1} (△) and 0.150 MPa s^{-1} (▽).

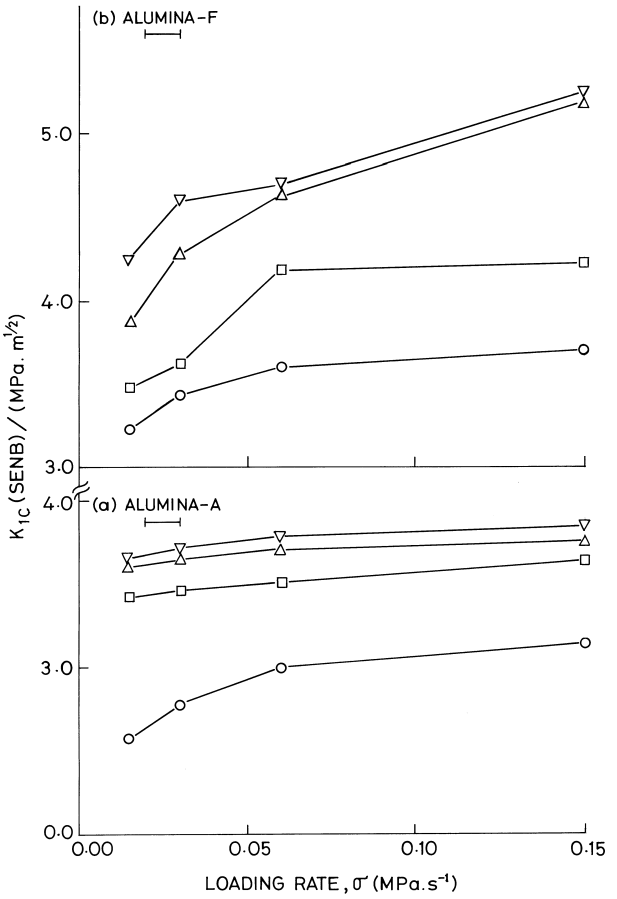

Fig. 6. Variation of K_{1c} (SENB) for alumina ceramics (a) alumina A, (b) alumina F; with loading rates in the range 0.015–0.150 MPa s^{-1} at different constant blade widths: 0.05 mm (○), 0.10 mm (□), 0.20 mm (△) and 0.30 mm (▽).

strength. This apparent increase in flexural strength could be again manifested in the apparent enhancement of K_{1c} with the loading rate, as is observed in the present work.

The data on variation of K_{1c} (SENB) with notch tip radius and normalised notch length are shown in Fig. 7 and Fig. 8 respectively, for alumina (A,D1,E,F) and SiC samples. Similar data for SSN samples (B,D) are shown in Fig. 9. K_{1c} (SENB) data of alumina, SiC (Fig. 7) and SSN [Fig. 9(a)], increase with notch tip radius or its square root. Pabst reported similar observations for alumina [31]. Higher tip radius occurs when a thicker blade is used to saw a notch. Now, a thicker blade is likely to cause more friction in the work piece than that caused by the thinner blade. This higher amount of friction may cause secondary crack formation ahead of the main notch tip. Under the externally applied stress, such secondary cracks are likely to grow along with main crack. As a result, crack branching can take place. The more the crack branching, higher would be the amount of additional energy dissipation. This should then be reflected in a higher rise in the K_{1c} value at larger

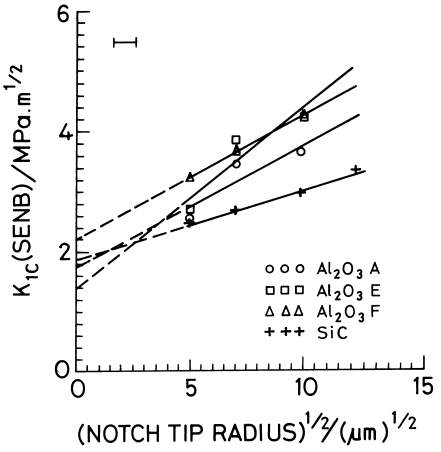

Fig. 7. Relationship between K_{1c} (SENB) and square root of notch tip radius in alumina and SiC ceramics.

notch tip radius, as is observed in the present work [Figs. 7 and 9(a)]. Extrapolated to zero notch tip radius, the present K_{1c} (SENB) data of alumina (E,F), SiC and SSN (B) samples compare favourably with the literature data where the K_{1c} values have been obtained on atomically sharp cracks [1,4,5,10,24].

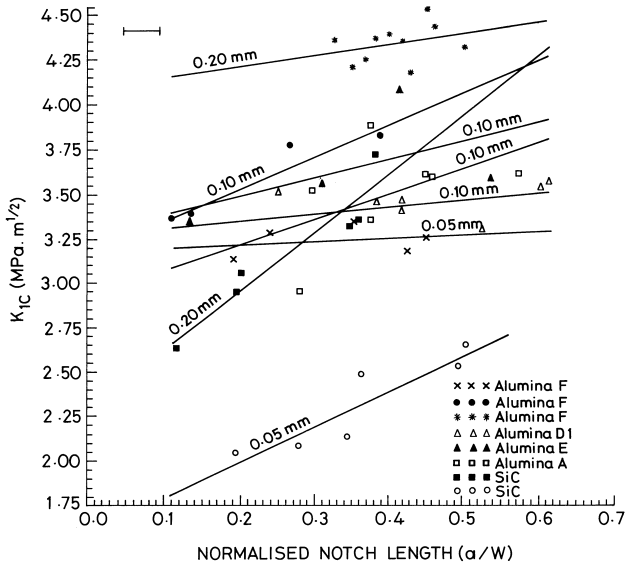

Fig. 8. Relationship between K_{1c} (SENB) and normalised notch length (a/W) in alumina and SiC ceramics at different constant blade widths (0.05–0.20 mm).

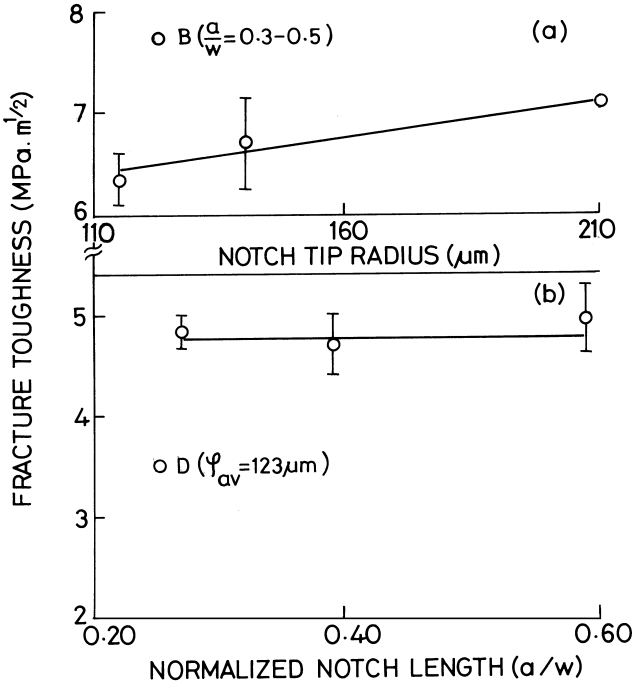

Fig. 9. Relationship between K_{1c} (SENB) and (a) notch tip radius and (b) normalised notch length (a/W), in SSN ceramics.

For a given constant width of blade, both alumina (A,D1,E,F) and SiC samples register a nominal increase in K_{1c} (SENB) with the normalised notch length ($a/W \sim$ 0.1–0.6) [Fig. 8]. However, for SSN there is no appreciable effect of a/W on K_{1c} (SENB), Fig. 9(b). Enhancement of K_{1c} (SENB) with the normalised notch length is believed to be linked to enhanced frictional interlocking of grains and adhesive forces at the crack surface [28,31,33]. If this is the case, then, increase in the normalised notch length will have a more profound effect on K_{1c} (SENB) of the coarse grained alumina (sample F) than that of the fine grained alumina (sample A). The observations of the present work [Fig. 8], match with this scenario.

4. Conclusions

The major conclusions of the present work are: (a) for alumina and SiC, K_{1c} (CNB) is always greater than K_{1c} (SENB) for a given blade width and a constant loading rate (0.015 M Pas^{-1}) (b) for sintered silicon nitride (SSN) ceramics, K_{1c} (SENB) is about 1.7 times higher than K_{1c} (IF) (c) for SSN ceramics, K_{1c} (FM) compares favourably with K_{1c} (SENB) in at least 80% of the cases investigated and (d) K_{1c} (SENB) of both alumina and SiC ceramics register an apparent increase with the normalised notch length, blade width, notch tip radius as well as the loading rate. Such effects are more pronounced in the coarse grained alumina than in the fine grained alumina. K_{1c} (SENB) data of SSN increase with the notch tip radius but remains insensitive to the variations in the normalised notch length in the range 0.3–0.6.

Acknowledgements

The authors appreciate the keen interests of Dr. C. Ganguly and Professor D. Munz and experimental assistance of Mr. Prabir Bhattacharyay in the present work.

References

[1] F.C. Chen, A.J. Ardell, Innovations in Materials Research 1 (1996) 47.
[2] A.S.F. Haubensak, J. Mat. Sc. 32 (1997) 1473.
[3] S. Gautier, E. Champion, D.B. Assollant, J. Eur. Ceram. Soc. 17 (1997) 1361.
[4] C. Anya, J. Mater. Sci. Lett. 16 (1997) 1300.
[5] A.K. Roy, S.K. Das, S. Maity, N.K. Mukhopadhyay, S. Dwarakadasa, E.S. Dwarakadasa, Interceram 46 (1997) 184.
[6] S. Li, L. Sun, H. Li, J. Li, Z. Wang, J. Mater. Sci. Lett. 16 (1997) 863.
[7] A.T. Zhender, C.-Y. Hui, E.D. Rodeghiero, J. Am. Cer. Soc. 80 (1997) 1319.
[8] T. Nojima, T. Oka, H. Kobayashi, J. Cer. Soc. Jap. 105 (1997) 690.
[9] R.W. Rice, J. Mater. Sci. 31 (1996) 4503.
[10] M.L.M. Kenane, Comp. Sc. Technol. 57 (1997) 597.
[11] D. Munz, in: R.C. Bradt, A.G. Evans, D.P.H. Hasselman, F.F. Lange (Eds.), Fracture Mechanics of Ceramics, vol. 6, Plenum Press, New York, 1983, pp. 1–26.
[12] S.W. Freiman, in: R.C. Bradt, A.G. Evans, D.P.H. Hasselman, F.F. Lange (Eds.), Fracture Mechanics of Ceramics, vol. 6, Plenum Press, New York, 1983, pp. 27–46.
[13] B. Mussler, M.V. Swain, N. Claussen, J. Am. Cer. Soc. 65 (1982) 566.
[14] G.K. Bansal, W.H. Duckworth, J. Mater. Sci. 13 (1978) 239.

[15] L.A. Simpson, I.G. Ritchie, D.J. Lloyd, J. Am. Cer. Soc. 58 (1975) 537.
[16] G. Popp, R.F. Pabst, J. Am. Cer. Soc. 64 (1981) C18.
[17] A.K. Mukhopadhyay, S.K. Datta, D. Chakraborty, Ceramics International 17 (1991) 335.
[18] W.F. Brown, J.E. Srawley, ASTM STP no. 410, 1966.
[19] G. Himsolt, T. Fett, K. Keller, D. Munz, Mater. Wissenschaften and Werkstoffteknik 20 (1989) 148.
[20] D. Munz, J.L. Shannon Jr., R.T. Bubsey, Int. J. Frac. 16 (1980) R137.
[21] W.S. Xian, ASTM STP no. 855, 1984, pp. 176–192.
[22] G.R. Anstis, P. Chantikul, B.R. Lawn, D.B. Marshall, J. Am. Cer. Soc. 64 (1981) 533.
[23] D. Chakraborty, A.K. Mukhopadhyay, Ceramics International 14 (1988) 127.
[24] A.K. Mukhopadhyay, S.K. Datta, D. Chakraborty, Ceramics International 17 (1991) 121.
[25] A.K. Mukhopadhyay, D. Chakraborty, J. Mukerji, J. Mater. Sci. Lett. 6 (1987) 1198.
[26] D. Chakraborty, A.K. Mukhopadhyay, Cent. Glass and Ceramic Res. Inst. Bull. 34 (1987) 59.
[27] D. Munz, R.T. Bubsay, J.L. Shannon Jr., J. Am. Cer. Soc. 63 (1980) 300.
[28] P. Lemaire, R. Piler, J. Mater. Sc. Lett. 7 (1988) 772.
[29] G.K. Bansal, J. Am. Cer. Soc. 59 (1976) 87.
[30] A.G. Evans, G. Tappin, Proc. Brit. Cer. Soc. 20 (1972) 275.
[31] R.F. Pabst, in: R.C. Bradt, D.P.H. Hasselman, F.F.Lange (Eds.), Fracture Mechanics of Ceramics, vol. 2, Plenum Press, New York, 1974, pp. 555–566.
[32] F.F. Buresch, in: R.C. Bradt, D.P.H. Hasselman, F.F. Lange (Eds.), Fracture Mechanics of Ceramics, vol. 4, Plenum Press, New York, 1978, pp. 835–847.
[33] R.F. Pabst, K. Kromp, G. Popp, Proc. Brit. Cer. Soc. 32 (1982) 89.